Sustainable Energy & Fuels

Light transfer through bubble-filled electrolyte for solar water splitting

Journal:	*Sustainable Energy & Fuels*
Manuscript ID	SE-ART-08-2022-001168.R2
Article Type:	Paper
Date Submitted by the Author:	04-Dec-2022
Complete List of Authors:	Bhanawat, Abhinav; University of California Los Angeles, Mechanical and Aerospace Engineering Pilon, Laurent; University of California Los Angeles, Mechanical and Aerospace Eng. Dept.

SCHOLARONE™
Manuscripts

Light transfer through bubble-filled electrolyte for solar water splitting

Abhinav Bhanawat and Laurent Pilon[+]

Mechanical and Aerospace Engineering Department

Henry Samueli School of Engineering and Applied Science

University of California, Los Angeles

[+]Corresponding Author: Phone: +1 (310)-206-5598, Fax: +1 (310)-206-2302

Engineering IV

420 Westwood Plaza, Los Angeles, CA 90095-1597

E-mail: pilon@seas.ucla.edu

December 3, 2022

Abstract

This study aims to systematically quantify the optical losses caused by hydrogen or oxygen bubbles released from an illuminated photoelectrode and rising through a semi-transparent aqueous electrolyte during photoelectrochemical water splitting. Indeed, the presence of gas bubbles increases backscattering of the incident radiation and absorption losses in the electrolyte due to multiple scattering. These optical losses were quantified by predicting (i) the normal-hemispherical reflectance, (ii) the electrolyte absorptance, and (iii) the area-averaged absorptance of the photoelectrode for wavelengths between 400 and 1100 nm using the Monte Carlo ray-tracing method. Results are reported for randomly distributed monodisperse and polydisperse bubbles with diameter ranging between 100 µm and 1 mm, volume fraction varying between 0 and 30%, and plume thickness ranging from 2 to 20 mm. The photoelectrode absorptance and efficiency were found to decrease with decreasing bubble diameter and increasing bubble volume fraction and plume thickness. In fact, without careful design and operation, the optical losses can significantly degrade the photoelectrode performance. The contribution to the total optical losses from bubbles attached to the photoelectrode surface increased with increasing bubble contact surface area coverage and decreasing plume thickness. The results indicate that increasing the bubble departure diameter by increasing the surface tension of the electrolyte/bubble interface and flowing the electrolyte to reduce the plume thickness can substantially minimize the optical losses. Additionally, illuminating the PEC cell from the anode side could be particularly beneficial given the larger size and smaller volume fraction of oxygen bubbles as compared to hydrogen bubbles.

Keywords: Photoelectrochemical water-splitting; PEC cell; Solar fuels; Bubbles; Optical losses; Hydrogen;

NOMENCLATURE

$\bar{A}$	Area-averaged absorptance
A	Absorptance
c	Speed of light in vacuum (m s^{-1})
D	Bubble diameter (mm)
d_c	Diameter of the contact circle (mm)
d_p	Projected diameter of the bubble (mm)
f_A	Projected surface area coverage (%)
f_s	Contact surface area coverage (%)
f_v	Volume fraction of bubbles (%)
h	Planck's constant (m^2 kg s^{-1})
H	Plume thickness (mm)
I	Incident light intensity ($Wm^{-2}s^{-1}$)
IQE	Internal quantum efficiency
$\bar{J}_{ph}$	Area-averaged photocurrent density generated in a photoelectrode (mA cm^{-2})
k	Absorption index
L	Length of the square photoelectrode (mm)
n	Refractive index
q	Charge of an electron (C)
R_{nh}	Normal-hemispherical reflectance

Greek symbols

λ	Wavelength of the incident radiation (nm)

ρ	Interface reflectance
θ_c	Contact angle (°)
γ	Surface tension (N m^{-1})
μ	Mean of lognormal size distribution
χ	Standard deviation of lognormal size distribution
σ	Standard deviation of normal size distribution (mm)

Subscripts

0	Bare photoelectrode
b	Bubble
e	Electrolyte
p	Photoelectrode

1 Introduction

Solar water splitting using photoelectrochemical (PEC) cells is a promising technology to store solar energy in the form of chemicals by direct conversion of water into H_2 and O_2 gases [1, 2]. A typical PEC cell comprises of a semiconductor photoelectrode and a counter electrode in a two-electrode configuration, separated by an ion-exchange membrane and immersed in an aqueous electrolyte [3]. Upon absorbing photons from sunlight, the photoelectrode generates electron-hole pairs that participate in the hydrogen evolution reaction (HER) at the cathode and in the oxygen evolution reaction (OER) at the anode. These redox reactions release gaseous products in the form of H_2 or O_2 bubbles that grow at nucleation sites on the photoelectrode surface [4]. When buoyancy forces exceed surface tension forces, the bubbles detach and rise through the electrolyte. However, the generated gas bubbles also scatter the incident light, causing optical losses [5].

The scattering losses from bubbles can be avoided if the photoelectrode is back-illuminated. However, the choice of illumination direction also depends on the photoelectrode's polarity, and on its minority carrier diffusion length. For example, $BiVO_4$ has typically poor electron transport and is usually back-illuminated when used as a photoanode for easier collection of photogenerated electrons [6]. However, many other photoelectrodes - made of TiO_2 or WO_3, for example - usually show higher photocurrent when front-illuminated [7, 8]. For bias-free water splitting, most configurations use a photoanode-photocathode tandem or a photoelectrode-PV tandem cell. In both configurations, the incident light inevitably interacts with either hydrogen or oxygen bubbles [3]. Such tandem cells are usually not illuminated from the PV side since the solar cell does not transmit light to the photoelectrode [9].

Overall, most PEC configurations incur optical losses from the presence of bubbles.

Recently, we quantified the effect of surface-attached spherical cap-shaped bubbles on optical losses in PEC cells consisting of large horizontal photoelectrodes immersed in a non-absorbing electrolyte and subjected to normally incident monochromatic radiation [10]. Monte Carlo ray-tracing method [11, 12] was used to predict the normal-hemispherical reflectance and the area-averaged and local absorptance of the photoelectrode in the visibile part of the solar spectrum for bubble contact angle θ_c varying between 0° and 180°, bubble diameter D ranging from 0.25 to 1.75 mm, and projected surface area coverage f_A varying from 0 to 78.5%. The bubble diameter and polydispersity were found to have no significant effect on the optical losses for a given projected surface area coverage f_A. However, the optical losses increased with increasing projected surface area coverage f_A due to stronger reflectance at the bubble/photoelectrode interface as compared to the electrolyte/photoelectrode interface. Three different optical regimes were defined by comparing the bubble contact angle θ_c and the critical angle θ_{cr} for total internal reflection at the electrolyte/bubble interface. The optical losses in each regime were based on the interplay of reflections at the electrolyte/bubble or the bubble/photoelectrode interface. In addition, the bubbles were found to significantly redistribute the incident light intensity causing most photons to be absorbed in a rim outside the projected footprint of the bubble attached to the photoelectrode surface. The study predicted optical losses up to 18% caused by bubbles with contact angle $\theta_c = 120°$, diameter $D = 1$ mm, and projected surface area coverage $f_A = 78.5\%$. Finally, hydrophilic photoelectrodes were recommended to reduce the bubble coverage on the photoelectrode which not only minimizes the optical losses but also increases the electrochemically active surface area of the photoelectrode.

Our previous study [10] was limited to the situation when bubbles were attached to the photoelectrode surface with no additional bubbles in the electrolyte volume. Such a scenario corresponds to the onset of water splitting reaction and/or to PEC cells having horizontal photoelelectrodes covered by a very thin layer of electrolyte. In all other configurations, the bubbles releasing from the photoelectrode surface and rising through the electrolyte also scatter the incident light until they burst at the free surface of the electrolyte or are convectively removed. Figure 1 shows the schematics of a photoelectrode in (a) vertical and (b) horizonal configuration, exposed to solar radiation through a bubble-filled electrolyte in a PEC cell. Figure 1(c) shows the photograph of a horizontal planar Si photoelectrode immersed in an aqueous electrolyte generating O_2 bubbles while being illuminated from the top [13]. Thus, for all photoelectrode orientations, the gas bubbles attached to the photoelectrode surface as well as those dispersed in the electrolyte scatter the incident light, resulting in optical losses.

The optics gets further complicated by light absorption by the aqueous electrolyte for incident radiation of wavelength $\lambda > 900$ nm. Döscher et al. [14] performed "detailed-balance" calculations based on Shockley-Queisser's method [15, 16] to estimate that the theoretical maximum solar-to-hydrogen (STH) conversion efficiency of a tandem PEC cell decreased from 40% to 25% due to sunlight absorption by bubble-free electrolyte of thickness 20 mm. However, the absorption losses may further increase due to light scattering by gas bubbles which increases the photon mean free path through the absorbing electrolyte.

This study aims to quantify systematically the optical losses in PEC cells due to light scattering by gas bubbles present in the electrolyte volume and due to light absorption by the semitransparent electrolyte. The parameters investigated included the bubble size

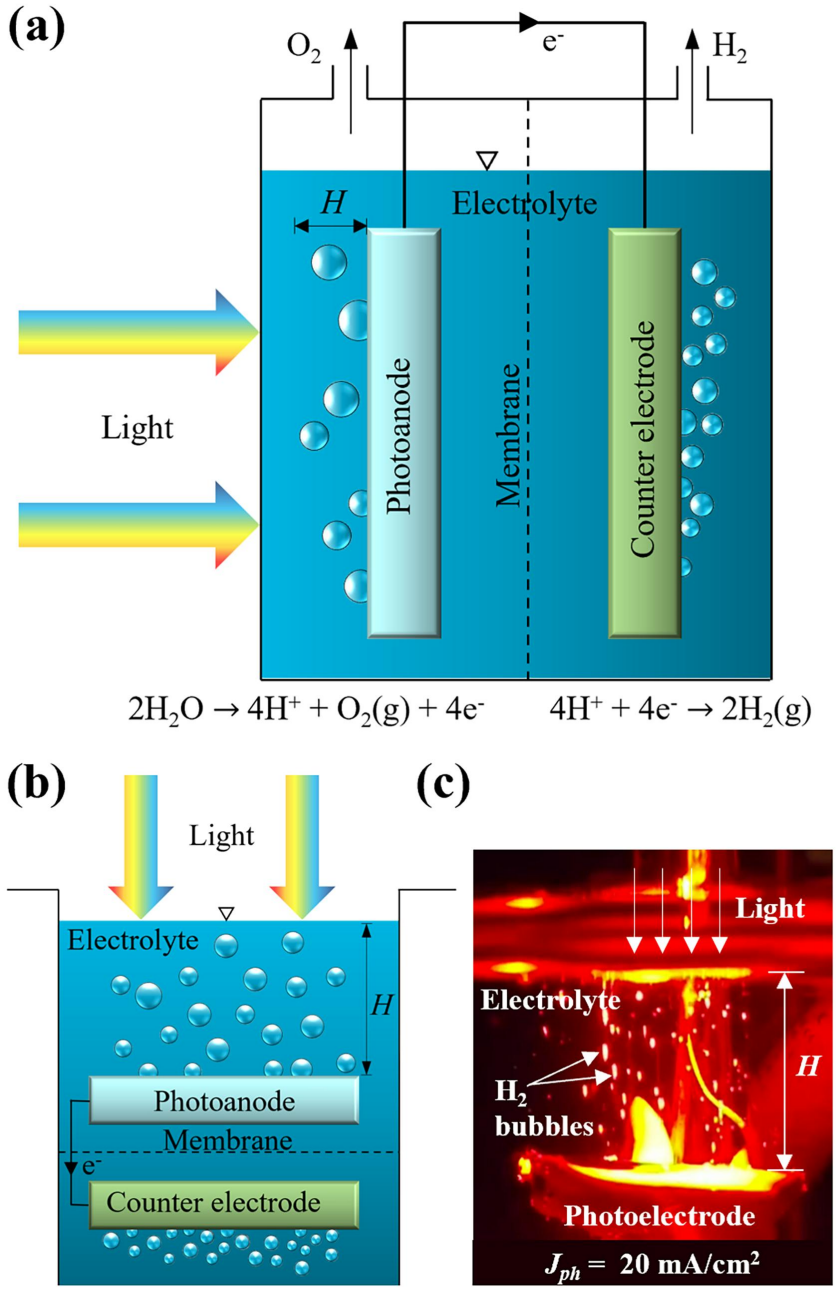

Figure 1: Schematic of light transfer to a (a) vertical and (b) horizontal photoelectrode in a PEC cell with a plume of gas bubbles of thickness H scattering the incident sunlight. (c) Photograph of hydrogen gas bubbles dispersed in the electrolyte covering a horizontal Si planar photoelectrode illuminated from the top (reprinted with permission from Ref. [13]. Copyright © 2021 Royal Society of Chemistry).

distribution and volume fraction, as well as the plume thickness. Spectral simulations were performed accounting for the variations in complex refractive indices of the Si photoelectrode and of the aqueous electrolyte. The contribution of the surface-attached bubbles to the total optical losses was also investigated. The results provide design guidelines to minimize bubble-induced optical losses and to enhance the performance of PEC cells.

2 Background

The effect of gas bubbles on light transfer in photoelectrochemical (PEC) cells remains relatively unexplored in the literature. Dorfi et al. [17] performed scanning photocurrent microscopy (SPCM) experiments using a normally incident laser beam emitting at wavelength 532 nm to quantify the photocurrent density losses associated with a single H_2 bubble attached to a horizontal Si photoelectrode. The losses were found to increase with increasing bubble diameter D, reaching up to 23% for $D = 1$ mm. A simple ray-tracing model based on Snell's law was used to explain the trends observed experimentally, without accounting for multiple reflections at the electrolyte/bubble and bubble/photoelectrode interfaces. However, the effects of bubbles dispersed in the electrolyte were not discussed.

Kempler et al. [13] studied experimentally the optical effects of H_2 or O_2 bubbles evolving from a horizontal Si photoelectrode of size 1×1 cm^2 immersed in a quiescent electrolyte and exposed to monochromatic radiation at 630 nm. The authors observed a decrease of around 10% in the photocurrent density due to the large bubble contact surface area coverage on the photoelectrode. The experimental findings were explained using ray-tracing simulations for a few monodisperse bubbles attached to the photoelectrode surface, but without accounting

for bubbles in the electrolyte. In addition, the exact thickness of the electrolyte layer covering the photoelectrode, the bubble volume fraction, and the contact surface area coverage were not reported.

Holmes-Gentle et al. [18] experimentally studied light scattering by a plume of O_2 gas bubbles rising from a transparent vertical electrode immersed in a quiescent electrolyte. The light source was a blue LED in the wavelength range 440-460 nm. The bubble diameter was estimated to be about 45 μm using digital imaging. The authors reported a decrease of about 5% in the normal-hemispherical transmittance of the electrode measured using an integrating sphere. Unfortunately, the plume thickness and the bubble volume fraction were not reported. Using the expression for scattering coefficient of a medium containing polydisperse particles as proposed by Curl [19], the authors suggested to minimize scattering losses by evolving fewer but larger bubbles and flowing the electrolyte laterally over the photoelectrode.

Njoka et al. [20] used high-speed imaging to characterize the H_2 and O_2 bubbles generated from vertical Pt electrodes immersed in an aqueous electrolyte in an electrochemical cell. The authors estimated the bubble plume thickness to be about 3 mm and the bubble departure diameter to be around 1.5 mm at a current density of 9.5 mA/cm^2 as the electrolyte was flowing at a velocity of around 2 mm/s. However, the bubble volume fraction was not reported. Next, they used the bubble characteristics obtained experimentally to perform Lorenz-Mie scattering simulations for wavelengths $\lambda = 400$, 500, and 650 nm. The authors estimated a drop of about 5% in the photocurrent density due to optical losses caused by the presence of bubbles. However, the exact bubble diameter, volume fraction, and plume thickness for which the optical losses were predicted were not specified, making them difficult

to reproduce. Furthermore, the presence of bubbles on the photoelectrode surface as well as reflections at the electrolyte/photoelectrode interface were not accounted for, thereby underestimating the optical losses.

Most previous studies [13,17,18] illuminated the photoelectrode with monochromatic light at a wavelength for which the aqueous electrolyte was transparent. Moreover, they provided limited discussion on the parameters responsible for the bubble-induced optical losses due to difficulties in controlling or characterizing the bubbles experimentally. Specifically, the effects of bubble volume fraction and plume thickness on the optical losses were not quantified. In practice, a higher photocurrent density in a PEC cell increases the gas generation rate, but it also increases the bubble volume fraction and thus the optical losses. In addition, horizontal photoelectrodes may incur more optical losses than vertical ones as bubbles occupy the entire electrolyte thickness (see Figure 1) resulting in multiple scattering of the incident light. Finally, the optical losses further increase due to light absorption by the aqueous electrolyte in the near-infrared portion of the solar spectrum.

The present study aims to systematically quantify the optical losses caused by gas bubbles forming at the photoelectrode surface and rising through the semitransparent electrolyte under normally incident sunlight. The Monte Carlo ray-tracing (MCRT) method was used to predict the area-averaged spectral absorptance of an infinitely large photoelectrode surface illuminated through a volume of electrolyte filled with randomly distributed monodisperse or polydisperse gas bubbles for a wide range of bubble diameter, volume fraction, and plume thickness. The predictions were systematically compared with those for a bare photoelectrode without any bubbles in the electrolyte. The results will be instrumental in optimizing the design and improving the performance of PEC cells for their envisioned outdoor opera-

tion.

3 Analysis

3.1 Problem statement and parametrization

Let us consider a square opaque Si photoelectrode of length L and complex index of refraction $m_{p,\lambda} = n_{p,\lambda} + ik_{p,\lambda}$ immersed in an aqueous electrolyte of complex index of refraction $m_{e,\lambda} = n_{e,\lambda} + ik_{e,\lambda}$. The photoelectrode is subjected to collimated and normally incident polychromatic light through a bubble plume of thickness H. The electrolyte volume contains N_v randomly distributed polydisperse spherical gas bubbles of diameter $(D_{v,i})_{1\leq i \leq N_v}$ following a normal size distribution $f(D)$, as illustrated in Figure 2. In addition, N_s polydisperse spherical cap-shaped bubbles having normal size distribution with diameter $(D_{s,j})_{1\leq j \leq N_s}$ and contact angle θ_c are attached to the photoelectrode surface with a contact surface area coverage f_s. The total volume fraction of the bubbles in the electrolyte and on the photoelectrode surface is denoted by f_v. The bubbles scatter light such that only a fraction of the incident light intensity is absorbed in the photoelectrode and converted into photocurrent, as accounted for by the photoelectrode's area-averaged spectral absorptance $\bar{A}_\lambda$. The remaining incident radiation is lost either by (i) backscattering, as quantified by the spectral normal-hemispherical reflectance $R_{nh,\lambda}$, or by (ii) absorption by the electrolyte, as represented by the spectral absorptance $A_{e,\lambda}$. Overall, an energy balance on the radiation incident on an opaque photoelectrode can be written as $R_{nh,\lambda} + A_{e,\lambda} + \bar{A}_\lambda = 1$. The objective of the present study is to quantify the bubble-induced optical losses in a PEC cell represented by $R_{nh,\lambda}$

and $A_{e,\lambda}$ and to assess the effects of bubble size distribution $f(D)$, volume fraction f_v, plume thickness H as well as contact surface area coverage f_s on the photoelectrode performance.

3.2 Assumptions

To make the problem mathematically trackable, the following assumptions were made: (1) dimensions of the photoelectrode and bubbles were much larger than the wavelength λ of the incident radiation so that geometric optics was valid and wave effects could be neglected. (2) All surfaces were optically smooth with specular reflection and refraction occurring at all interfaces according to Snell's law and Fresnel's equations. (3) Reflection at the top boundary of the computational domain was ignored. (4) Gas bubbles were spherical and randomly distributed in the electrolyte volume. (5) Gas bubbles attached to the photoelectrode surface were spherical cap-shaped and randomly distributed with constant volume and constant contact angle θ_c. (6) The gas inside the bubbles was transparent with $n_{b,\lambda} = 1.0$. (7) The photoelectrode was opaque so that all photons transmitted through the photoelectrode surface were absorbed. (8) The bubble plume thickness H was the same over the entire photoelectrode surface. (9) The thickness of the semitransparent electrolyte layer covering the photoelectrode was equal to the bubble plume thickness H.

3.3 Computational bubble generation

Monodisperse or polydisperse spherical bubbles having normal size distribution with mean diameter $\bar{D}$ and standard deviation σ were computationally generated and randomly distributed in the electrolyte volume following a procedure based on our previous study [10].

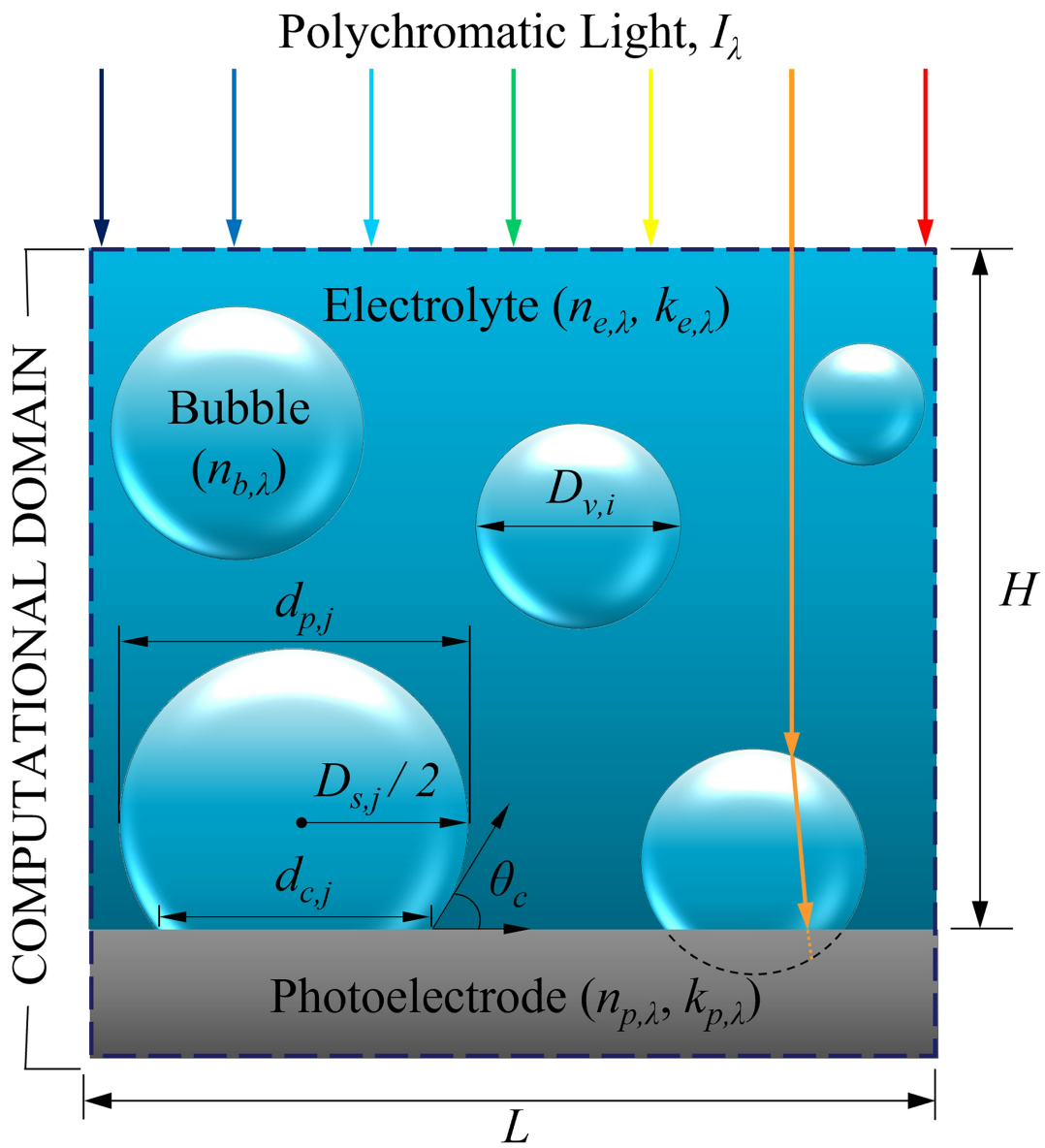

Figure 2: Side view of the 3D computational domain considered in this study showing polydisperse spherical bubbles of diameter $(D_{v,i})_{1\leq i\leq N_v}$ dispersed in the electrolyte volume and cap-shaped bubbles of diameter $(D_{s,j})_{1\leq j\leq N_s}$ attached to the photoelectrode surface with contact angle θ_c. Rays reaching a location below the photoelectrode surface, e.g., orange ray, were retraced and either reflected or refracted at the bubble/photoelectrode interface.

First, random bubble diameters were generated in accordance with the imposed size distribution until their total volume fraction in the electrolyte reached the desired value. Then, the bubbles were assigned random center locations (x_i, y_i, z_i) while ensuring that they did not overlap and were confined within the electrolyte volume. The corresponding volume fraction f_v for bubbles dispersed in the electrolyte is expressed as

$$f_v = \left(\sum_{i=1}^{N_v} \frac{\pi}{6} D_{v,i}^3 \right) / HL^2, \tag{1}$$

where N_v is the number of bubbles dispersed in the electrolyte volume, $D_{v,i}$ is the diameter of the ith bubble, H is the bubble plume thickness, and L is the length of the square photoelectrode.

To simulate the presence of spherical cap-shaped bubbles on the photoelectrode surface, in addition to those in the electrolyte volume, spherical bubbles satisfying an imposed volume fraction were computationally generated and randomly distributed, as previously described. However, this time, the bubbles were allowed to intersect the bottom surface of the electrolyte domain. The resulting cap-shaped bubbles were identified and moved perpendicularly to the bottom surface to achieve the desired bubble contact angle θ_c. Then, the total volume fraction f_v of bubbles comprising (i) N_s spherical cap-shaped bubbles of diameter $(D_{s,j})_{1\leq j \leq N_s}$ and contact angle θ_c attached to the photoelectrode surface and (ii) N_v spherical bubbles of diameter $(D_{v,i})_{1\leq i \leq N_v}$ in the electrolyte volume is given by

$$f_v = \left[\sum_{i=1}^{N_v} \frac{\pi}{6} D_{v,i}^3 + \sum_{j=1}^{N_s} \frac{\pi}{24} D_{s,j}^3 (2 + 3cos\theta_c - cos^3\theta_c) \right] / HL^2. \tag{2}$$

Moreover, the projected surface area coverage f_A of bubbles attached to the photoelectrode

surface is given by

$$f_A = \left(\sum_{j=1}^{N_s} \frac{\pi}{4} d_{p,j}^2 \right) / L^2, \tag{3}$$

where $d_{p,j}$ is the projected diameter of the jth cap-shaped bubble defined as $d_{p,j} = D_{s,j}$ for $0° \leq \theta_c < 90°$ and $d_{p,j} = D_{s,j}\sin\theta_c$ for $90° \leq \theta_c < 180°$. Similarly, the bubble contact surface area coverage f_s on the photoelectrode can be defined as

$$f_s = \left(\sum_{j=1}^{N_s} \frac{\pi}{4} d_{c,j}^2 \right) / L^2, \tag{4}$$

where $d_{c,j}$ is the diameter of the contact circle of the jth cap-shaped bubble given by $d_{c,j} = d_{p,j}\sin\theta_c$ for $\theta_c \leq 90°$, and $d_{c,j} = d_{p,j}$ for $\theta_c > 90°$.

3.4 Closure laws

Spectral simulations were performed over wavelengths ranging between 300 nm and 3 µm encompassing the solar spectrum. The spectral refractive $n_{e,\lambda}$ and absorption $k_{e,\lambda}$ indices of the aqueous electrolyte were assumed to be that of water reported in Ref. [21]. The photoelectrode material was chosen to be crystalline undoped Si whose spectral refractive $n_{p,\lambda}$ and absorption $k_{p,\lambda}$ indices were obtained from Ref.[22].

Unless otherwise noted, monodisperse bubbles of diameter $D = 1$ mm were simulated based on the values reported in the literature [17,20] and also based on the bubble departure diameter of 1.14 mm at STP predicted by Fritz correlation [23] for a hydrophilic surface with contact angle $\theta_c = 20°$. However, when studying the effect of monodisperse bubble diameter, D was taken as either 0.1, 0.3, 0.5, or 1 mm. The effect of polydispersity was also analyzed by using normally distributed bubble diameters with a mean value $\bar{D} = 1$ mm and standard deviation $\sigma = 0.25$ mm with bubble diameter $D_{v,i}$ such that $\bar{D} - 3\sigma < D_{v,i} < \bar{D} + 3\sigma$.

The bubble volume fraction f_v ranged between 0 and 30% corresponding to the bubbly flow regime [23]. Typically, the bubble volume fraction encountered in water electrolysis varies between 0 and 12% [4]. The bubble plume thickness H varied between 2 and 20 mm according to the typical electrolyte thicknesses used in photoelectrochemical cells [14]. The length of the square photoelectrode was $L = 10$ mm with periodic boundary conditions, unless otherwise noted.

3.5 Methods of solution

3.5.1 Light transfer

The Monte Carlo ray-tracing method [11, 12] was used to predict the normal-hemispherical reflectance $R_{nh,\lambda}$, the electrolyte absorptance $A_{e,\lambda}$, and the area-averaged absorptance $\bar{A}_\lambda$ of the opaque photoelectrode subjected to normally incident light through a bubble-filled semitransparent electrolyte volume. Collimated photon bundles or "rays" were incident on the computational domain assuming periodic boundary conditions such that the rays reaching any of the four sides of the computational domain re-entered from the opposite side at the same height and in the same direction. The rays were traced until they were either absorbed in the photoelectrode or in the electrolyte, or were backscattered out from the top of the computational domain. The computational steps for each ray are listed in Supplementary Material.

All the simulations were performed with a total number of incident photon bundles equal to 10^7 necessary to achieve numerical convergence [24]. In order to validate the Monte Carlo ray-tracing (MCRT) code, three cases for which the analytical expressions of the

photoelectrode absorptance were known were simulated (see Supplementary Material).

3.5.2 Bubble-induced optical losses

First, the area-averaged photoelectrode absorptance $\bar{A}_\lambda$ was normalized with the absorptance $\bar{A}_{0,\lambda}$ of a photoelectrode in the absence of bubbles. The latter can be written as [11]

$$\bar{A}_{0,\lambda} = (1 - \rho_{ep,\lambda})e^{-\kappa_{e,\lambda}H} \tag{5}$$

where H is the thickness (in m) of semitransparent electrolyte covering the photoelectrode, $\kappa_{e,\lambda} = 4\pi k_{e,\lambda}/\lambda$ is the absorption coefficient of the electrolyte (in m^{-1}), and $\rho_{ep,\lambda}$ is the reflectance at the optically smooth interface between the electrolyte and the photoelectrode such that [11]

$$\rho_{ep,\lambda} = \frac{(n_{e,\lambda} - n_{p,\lambda})^2 + (k_{e,\lambda} - k_{p,\lambda})^2}{(n_{e,\lambda} + n_{p,\lambda})^2 + (k_{e,\lambda} + k_{p,\lambda})^2}. \tag{6}$$

Then, the bubble-induced optical losses (%) were given by (1 - $\bar{A}_\lambda/\bar{A}_{0,\lambda}$).

3.5.3 Photoelectrode efficiency limit

A photoelectrode immersed in an electrolyte behaves in a similar way as a solar cell due to the formation of a semiconductor-electrolyte junction that separates the photogenerated charge carriers [25]. However, the maximum possible efficiency of a photoelectrode is always smaller than or equal to that of a photovoltaic (PV) solar cell made from the same semiconductor and operating at its maximum power point (MPP) due to the photovoltage of 1.23 V required for driving the water splitting reaction [25, 26]. The equality only holds for semiconductors that generate photovoltage exactly equal to 1.23 V at STP. The more commonly cited solar-to-hydrogen (STH) efficiency is only applicable to photoelectrodes if they can generate the

photovoltage required for water splitting and compensate for overpotential losses [25, 26]. Here, we used PV efficiency to quantify the impact of bubbles since it corresponds to the upper bound of the photoelectrode efficiency for a given material.

Holmes-Gentle et al. [27] developed an open-source computational tool to predict the PV efficiency limit of a semiconductor based on the detailed-balance model first proposed by Shockley and Quiesser [15]. The model accounts for the spectral irradiance of sunlight and recombination losses. However, it neglects light absorption in the electrolyte and backscattering by the bubbles and photolelectrode surface. Here, we incorporate these optical losses and predict the maximum PV efficiency to quantify the deleterious effect of bubbles on the performance of a photoelectrode. To do so, spectral simulations in wavelength intervals of 10 nm were performed over 1 Sun AM 1.5G reference spectrum, according to standard ASTM G173-3, for different volume fractions f_v and plume thicknesses H considering only bubbles dispersed in the electrolyte. Then, the spectral solar irradiance was multiplied by the photoelectrode's spectral absorptance predicted from MCRT simulations. Finally, the spectral solar flux absorbed in the photoelectrode was used as input into the open-source tool developed by Holmes-Gentle et al. [27] to predict the PV efficiency limit of a Si photoelectrode having a band gap of 1.12 eV.

4 Results and discussion

This section presents the effects of (1) bubble size distribution $f(D)$, (2) volume fraction f_v, (3) plume thickness H, and (4) surface area coverage f_s on the normal-hemispherical reflectance $R_{nh,\lambda}$, electrolyte absorptance $A_{e,\lambda}$, and area-averaged absorptance $\bar{A}_\lambda$ of a Si

photoelectrode. First, the photoelectrode surface was assumed to be free of cap-shaped bubbles so that $f_s = 0\%$ and bubbles were only present in the electrolyte volume. Then, the effect of surface-attached cap-shaped bubbles on the overall optical losses was quantified. In all cases, the normalized area-averaged absorptance $\bar{A}_\lambda/A_{0,\lambda}$ was used to compare the spectral optical losses in a PEC cell with and without bubbles for given bubble diameter D, volume fraction f_v, and plume thickness H.

4.1 Effect of bubble size distribution

Figures 3(a) and 3(b) respectively plot the spectral normal-hemispherical reflectance $R_{nh,\lambda}$ and area-averaged photoelectrode absorptance $\bar{A}_\lambda$ as functions of wavelength λ for monodisperse bubbles of diameter $D = 1$ mm or polydisperse bubbles with either normal size distribution with mean diameter $\bar{D} = 1$ mm and standard deviation $\sigma = 0.25$ mm, or lognormal size distribution with mean $\mu = 0.05$ and standard deviation $\chi = 0.25$ (see Figure S3). The probability density functions for the normal $f_n(D)$ and lognormal size distribution $f_{ln}(D)$ are respectively expressed as

$$f_n(D) = \frac{1}{\sigma\sqrt{2\pi}} e^{-\frac{1}{2}\left(\frac{D-\bar{D}}{\sigma}\right)^2} \; and \; f_{ln}(D) = \frac{1}{D\chi\sqrt{2\pi}} e^{\left(-\frac{(\ln D-\mu)^2}{2\chi^2}\right)}. \tag{7}$$

Here, the bubble volume fraction f_v was either 10% or 20% and the bubble plume thickness H was 10 mm. Predictions for a photoelectrode immersed in the electrolyte without any bubbles (i.e., $f_v = 0\%$) are also shown as references. Figure 3 establishes that the presence of bubbles in the electrolyte increased the reflection losses and decreased light absorption in the photoelectrode.

In addition, for a given volume fraction f_v, bubble polydispersity led to a slightly smaller

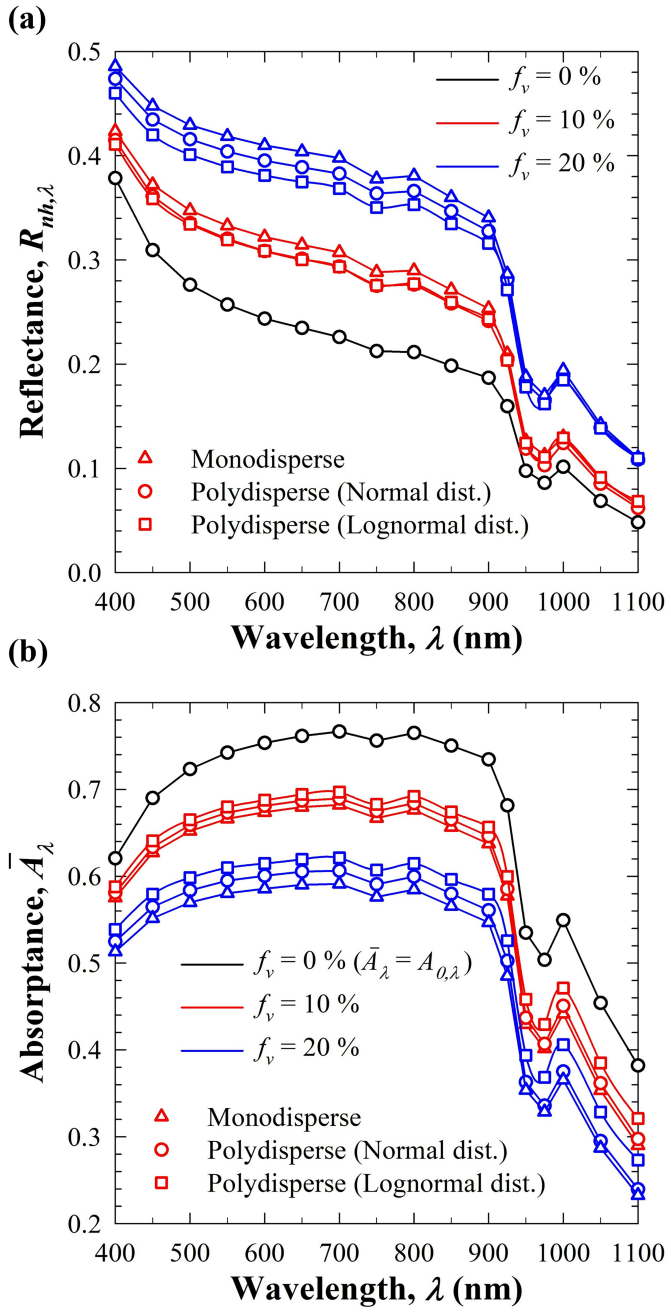

Figure 3: Comparison of (a) spectral normal-hemispherical reflectance $R_{nh,\lambda}$ and (b) spectral area-averaged photoelectrode absorptance $\bar{A}_\lambda$ for either monodisperse bubbles or polydisperse bubbles with normal or lognormal size distribution for mean bubble diameter of 1 mm and bubble volume fractions f_v of 10% or 20%.

reflectance $R_{nh,\lambda}$ and a larger photoelectrode absorptance $\bar{A}_\lambda$ compared to when the bubbles were monodisperse with the same mean diameter. However, these observations were less pronounced for $\lambda > 900$ nm, when both $R_{nh,\lambda}$ and $\bar{A}_\lambda$ decreased substantially due to light absorption by the aqueous electrolyte. In fact, for a given volume fraction f_v and mean bubble diameter $\bar{D} = 1$ mm, the relative difference between the predictions of $R_{nh,\lambda}$ and $\bar{A}_\lambda$ for polydisperse and monodisperse bubbles was less than 5% at all wavelengths despite a relatively wide bubble size distribution. In addition, spectral predictions for lognormal and normal size distributions were similar for the same mean diameter and range of bubble diameters for all wavelengths. Figures S4(a) and S4(b) show similar trends for smaller polydisperse bubbles having either normal size distribution with mean diameter $\bar{D} = 300$ µm and standard deviation $\sigma = 75$ µm, or lognormal distribution for diameters (in mm) with mean $\mu = -1.14$ and standard deviation $\chi = 0.24$. Figure S5 compares the probability density functions for these two size distributions. Thus, the bubble volume fraction f_v and mean diameter $\bar{D}$ had a dominant effect on $R_{nh,\lambda}$ and $\bar{A}_\lambda$ while the bubble polydispersity had a secondary effect.

Figures S6(a) and S6(b) plot the spectral normal-hemispherical reflectance $R_{nh,\lambda}$ and area-averaged photoelectrode absorptance $\bar{A}_\lambda$ as functions of wavelength λ for normally distributed polydisperse bubbles with mean diameter $\bar{D} = 0.3$ or 1 mm for volume fraction $f_v = 10\%$. Here, the standard deviation σ was taken as 0, $\bar{D}/4$, or $\bar{D}/2$ and the bubble diameters were considered in the range $\bar{D} - 2\sigma < D < \bar{D} + 2\sigma$. Figure S6 shows that the standard deviation had a more pronounced effect on the predictions for bubbles with smaller mean diameter. Overall, the effect of bubble polydispersity should be accounted for, particularly when the bubbles are small.

4.2 Effect of bubble diameter D

Figure 4(a) presents the normalized area-averaged photoelectrode absorptance $\bar{A}_\lambda/\bar{A}_{0,\lambda}$ as a function of wavelength λ for bubble diameters $D = 0.1$, 0.3, 0.5, and 1 mm for volume fraction $f_v = 10\%$ and plume thickness $H = 10$ mm. It indicates that the spectral variation of $\bar{A}_\lambda/\bar{A}_{0,\lambda}$ followed a similar trend for all bubble diameters i.e., a slight decrease in magnitude as λ increased from 400 to 900 nm, and a substantial decrease beyond 900 nm. However, the drop was not as sharp as that seen for absorptance $\bar{A}_\lambda$ in Figure 3 because the normalization factor $\bar{A}_{0,\lambda}$ accounts for the significant light absorption by the aqueous electrolyte even in the absence of bubbles.

Figure 4(a) also shows that the photoelectrode absorptance decreased sharply with decreasing bubble diameter. In fact, for $f_v = 10\%$ and $H = 10$ mm, the optical losses for bubble diameter $D = 100$ µm were nearly 5 times larger than those for diameter $D = 1$ mm for all wavelengths considered. To identify the different underlying mechanisms, Figure 4(b) plots the corresponding normal-hemispherical reflectance R_{nh}, the electrolyte absorptance A_e, and the area-averaged photoelectrode absorptance $\bar{A}$ as functions of bubble diameter D at wavelength $\lambda = 950$ nm when absorption by the electrolyte was significant. It indicates that the photoelectrode absorptance $\bar{A}$ decreased with decreasing bubble diameter primarily due to large reflection losses caused by multiple scattering from a large number of bubbles. On the other hand, the electrolyte absorption losses remained nearly constant and independent of bubble diameter since absorption is a volumetric phenomenon and the total electrolyte volume remained constant for given values of volume fraction f_v and plume thickness H.

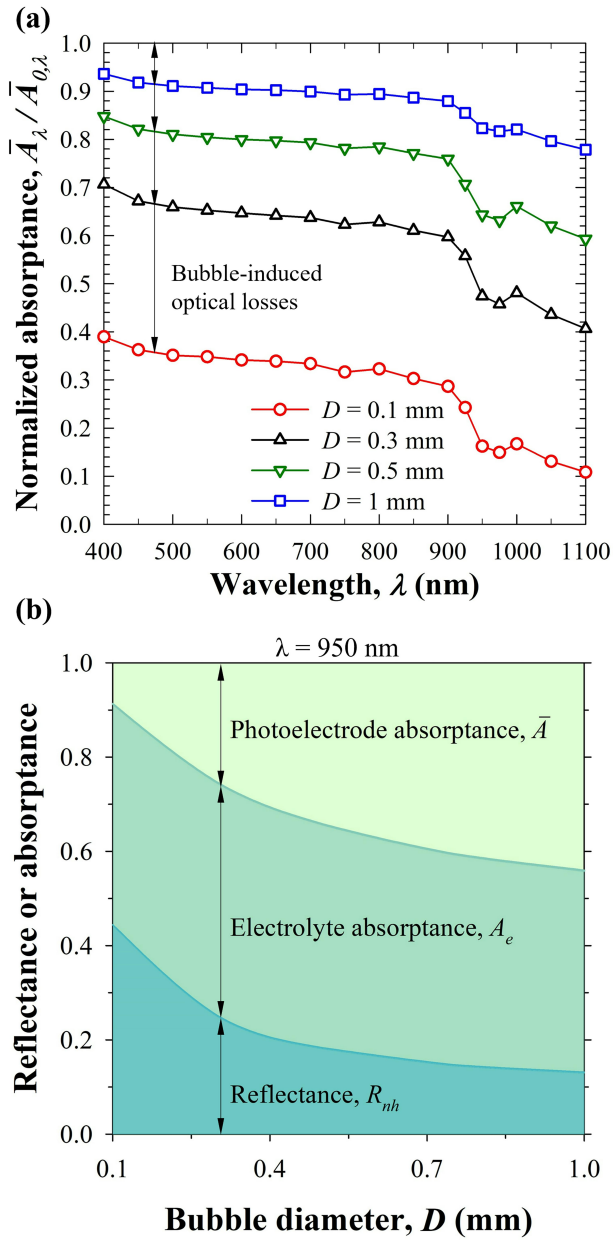

Figure 4: (a) Normalized area-averaged photoelectrode absorptance $\bar{A}_\lambda/\bar{A}_{0,\lambda}$ as a function of wavelength for different bubble diameters. (b) Normal-hemispherical reflectance R_{nh}, electrolyte absorptance A_e, and area-averaged photoelectrode absorptance $\bar{A}$ as functions of bubble diameter D at wavelength $\lambda = 950$ nm. In all cases, the bubble volume fraction was $f_v = 10\%$ and the plume thickness was $H = 10$ mm.

4.3 Effect of bubble volume fraction f_v

Figure 5(a) plots the normalized area-averaged photoelectrode absorptance $\bar{A}_\lambda/\bar{A}_{0,\lambda}$ as a function of wavelength λ for bubble volume fractions f_v = 5%, 10%, 20%, and 30% for bubble diameter D = 1 mm and plume thickness H = 10 mm. Here, the spectral variation of normalized absorptance $\bar{A}_\lambda/\bar{A}_{0,\lambda}$ was similar to that in Figure 4(a) for all volume fractions considered. Interestingly, Figure 5(a) shows that light absorption in the photoelectrode decreased substantially with increasing bubble volume fraction f_v. In fact, the bubble-induced optical losses for f_v = 30% reached as high as 30% in the visible, and up to 50% at wavelength λ = 1100 nm when the electrolyte was semitransparent. This indicates that, in practice, a high gas generation rate in PEC cells, which results in large bubble volume fraction, also leads to large optical losses. In turn, the generated photocurrent density decreases, as well as the gas generation rate and the bubble volume fraction. Such an oscillatory behavior, caused by light scattering by generated bubbles, may lead to oscillating photocurrent observed in chronoamperometry experiments [17].

Figure 5(b) presents the normal-hemispherical reflectance R_{nh}, the electrolyte absorptance A_e, and the area-averaged photoelectrode absorptance $\bar{A}$ as functions of bubble volume fraction f_v for diameter D = 1 mm and plume thickness H = 10 mm at wavelength λ = 950 nm. It establishes that the photoelectrode absorptance decreased significantly with increasing volume fraction f_v due to increasing reflection losses and high absorption losses. On one hand, the reflectance R_{nh} increased monotonously with f_v due to backscattering and multiple scattering by the increasing number of bubbles. On the other hand, the electrolyte absorptance A_e first increased slightly and then plateaued with increasing f_v, which can

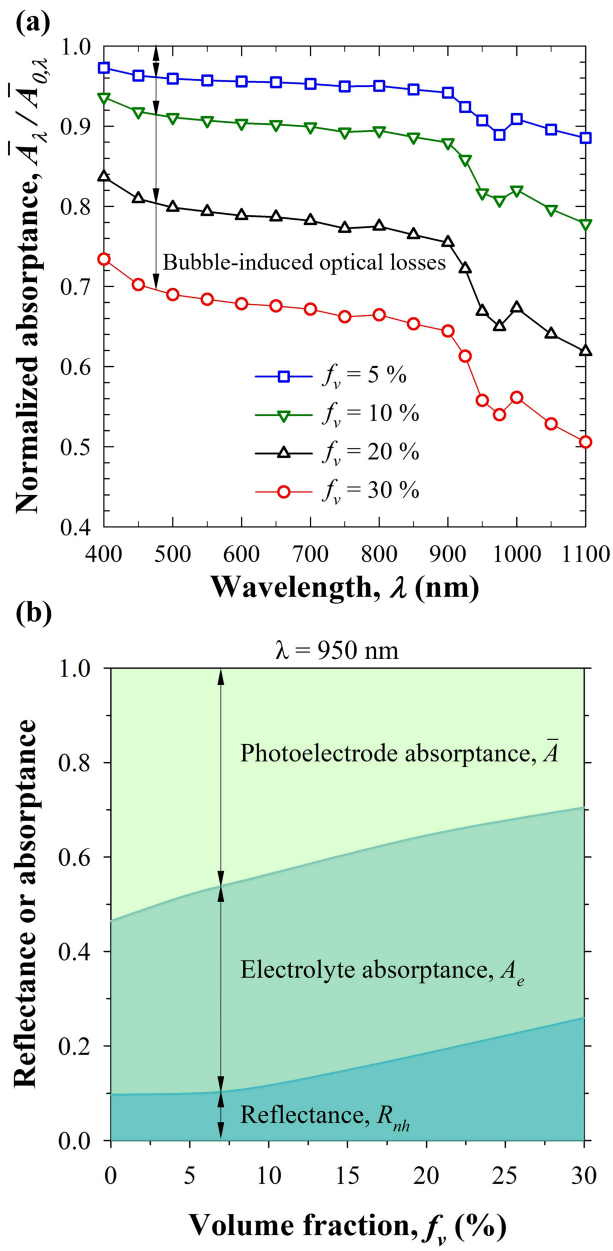

Figure 5: (a) Normalized area-averaged photoelectrode absorptance $\bar{A}_\lambda/\bar{A}_{0,\lambda}$ as a function of wavelength for different volume fractions. (b) Normal-hemispherical reflectance R_{nh}, electrolyte absorptance A_e, and area-averaged photoelectrode absorptance $\bar{A}$ as functions of bubble volume fraction f_v at wavelength $\lambda = 950$ nm. In all cases, the bubble diameter was $D = 1$ mm and the plume thickness was $H = 10$ mm.

be attributed to the interplay between increasing mean free path of scattered photons and decreasing electrolyte volume.

The trends presented in this study show good qualitative agreement with experimental results reported in Refs. [13, 18] showing larger optical losses at higher gas generation rates. However, a direct comparison of results was not possible owing to a lack of reported bubble volume fraction and plume thickness. Nonetheless, the optical losses predicted in this study remained less than 10% for volume fractions $f_v < 10\%$, in agreement with the results reported experimentally [13, 18].

4.4 Effect of bubble plume thickness H

Figure 6(a) plots the normalized area-averaged photoelectrode absorptance $\bar{A}_\lambda/\bar{A}_{0,\lambda}$ as a function of wavelength λ for bubble plume thicknesses H = 2, 5, 10, and 20 mm for bubble diameter D = 1 mm and volume fraction $f_v = 10\%$. It indicates that the spectral variation of normalized absorptance $\bar{A}_\lambda/\bar{A}_{0,\lambda}$ was similar to those in Figures 4(a) and 5(a) for all thicknesses. Figure 6(a) also shows that the normalized absorptance $\bar{A}_\lambda/\bar{A}_{0,\lambda}$ decreased substantially with increasing thickness for all wavelengths. For $\lambda < 900$ nm, absorption by the electrolyte remained negligible, while the reflection losses increased with increasing plume thickness (see Figure S10(a)) due to backscattering and multiple scattering. Interestingly, the reflectance R_{nh} decreased with increasing plume thickness H for all $\lambda > 900$ nm because the scattered radiation was more likely to be absorbed in the semitransparent electrolyte volume than to be backscattered. The same observations can be made in Figure 6(b) plotting the normal-hemispherical reflectance R_{nh}, the electrolyte absorptance A_e, and the area-averaged

photoelectrode absorptance $\bar{A}$ as functions of bubble plume thickness H for diameter $D =$ 1 mm and volume fraction $f_v = 10\%$ at wavelength $\lambda = 950$ nm.

4.5 Effect of additional bubbles on photoelectrode surface

This section aims to assess the contribution of cap-shaped bubbles attached to the photoelectrode surface to the total optical losses. The bubble contact angle was taken as $\theta_c = 90°$ to maximize the bubble contact surface area coverage f_s and achieve large backscattering [10].

4.5.1 Effect of contact surface area coverage f_s

Figures 7(a) plots the normalized area-averaged photoelectrode absorptance $\bar{A}_\lambda/\bar{A}_{0,\lambda}$ as a function of wavelength λ for bubble diameter $D = 1$ mm, plume thickness $H = 10$ mm, and volume fraction $f_v = 5\%$, 19.3%, and 28.3%, while the contact surface area coverage f_s was respectively equal to 3.1%, 25.1%, and 47.1%. Note that the contact surface area coverage f_s increased with increasing bubble volume fraction f_v in qualitative agreement with experimental observations. Results for a bare photoelectrode such that $f_s = 0\%$ at different volume fractions f_v are also shown as references. Figure 7(a) establishes that the surface-attached bubbles further increased the optical losses by up to 6% as compared to a bare photoelectrode for $f_v = 28.3\%$. These additional optical losses increased with increasing contact surface area coverage f_s due to the larger reflectance of the bubble/photoelectrode interface compared to the electrolyte/photoelectrode interface. Thus, Figure 7(a) confirms that the use of hydrophilic photoelectrodes reduces the optical losses.

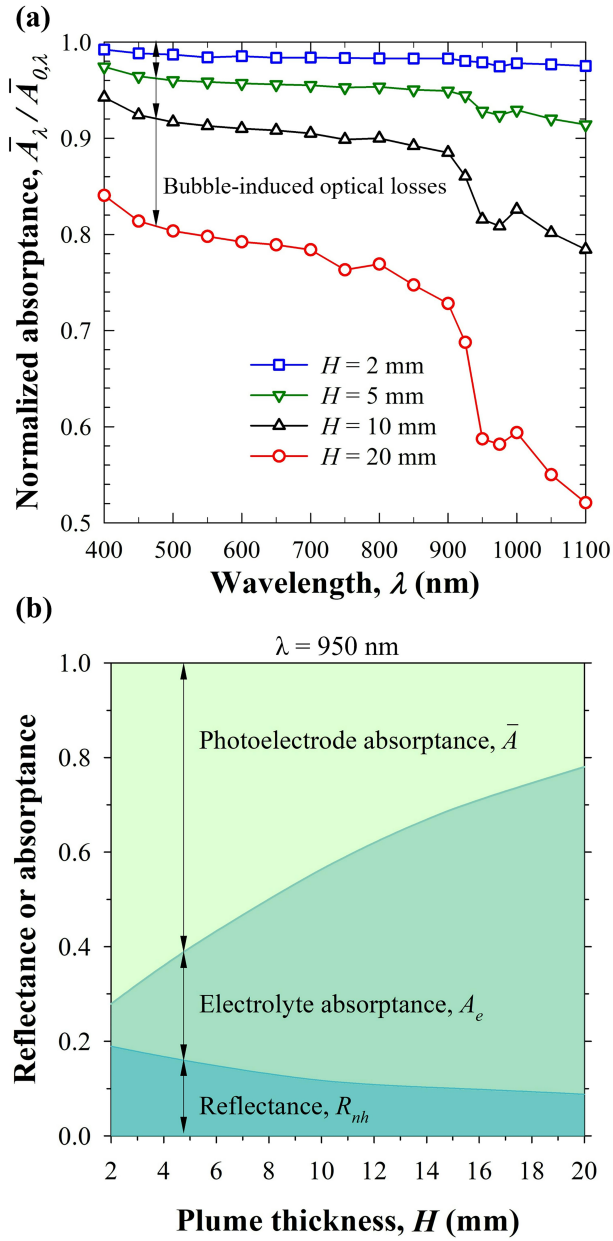

Figure 6: (a) Normalized area-averaged photoelectrode absorptance $\bar{A}_\lambda/\bar{A}_{0,\lambda}$ as a function of wavelength for different bubble plume thicknesses. (b) Normal-hemispherical reflectance R_{nh}, electrolyte absorptance A_e, and area-averaged photoelectrode absorptance $\bar{A}$ as functions of bubble plume thickness H at wavelength $\lambda = 950$ nm. In all cases, the bubble diameter was $D = 1$ mm and the volume fraction was $f_v = 10\%$.

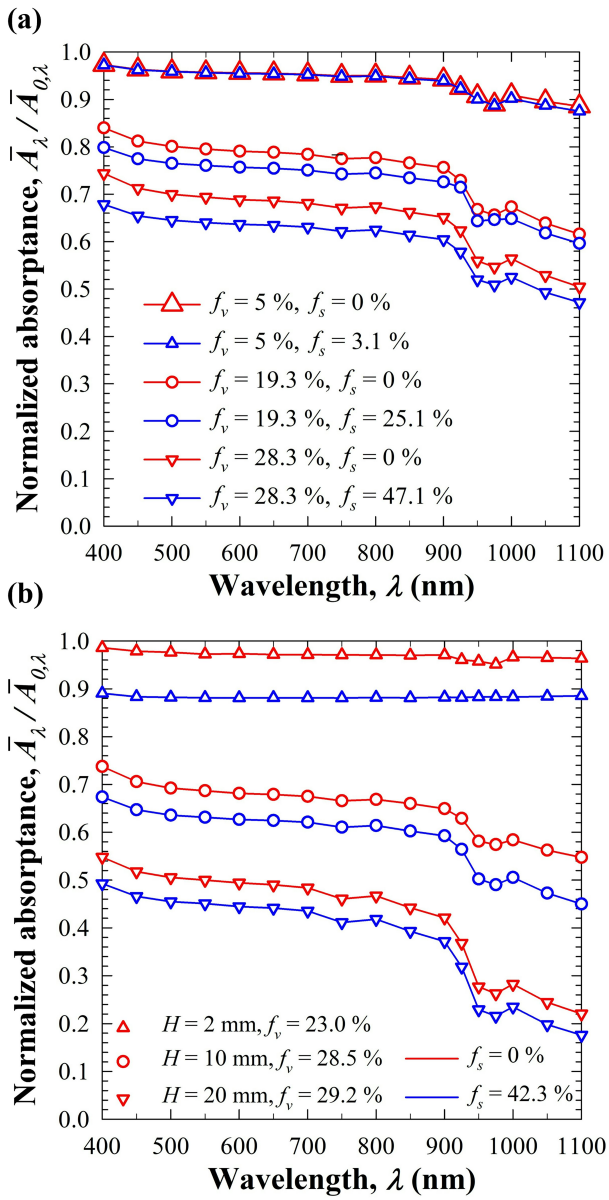

Figure 7: (a) Normalized area-averaged photoelectrode absorptance $\bar{A}_\lambda/\bar{A}_{0,\lambda}$ as functions of wavelength for (a) different bubble contact surface area coverages f_s for plume thicknesses H = 10 mm, and (b) different plume thicknesses for f_s = 22.0%. The results for f_s = 0% for the same volume fraction f_v are also presented. In all cases, the bubble diameter was D = 1 mm.

4.5.2 Effect of plume thickness H

Figure 7(b) presents the normalized area-averaged photoelectrode absorptance $\bar{A}_\lambda/\bar{A}_{0,\lambda}$ as a function of wavelength λ for bubble plume thicknesses $H = 2$, 10, and 20 mm for bubble contact angle $\theta_c = 90°$, contact surface area coverage $f_s = 42.3\%$, and bubble diameter $D = 1$ mm. Again, the results were compared with those for the same volume fraction but with $f_s = 0\%$. Figure 7(b) indicates that the absolute difference between the predictions for $f_s = 0\%$ and $f_s = 42.3\%$ decreased from about 10% at $H = 2$ mm to less than 4% for $H = 20$ mm. This can be attributed to the reduced photon flux reaching the bubble-covered photoelectrode due to backscattering by the bubbles dispersed in the electrolyte. In other words, the effect of surface-attached bubbles on the overall optical losses decreased with increasing plume thickness H. Thus, photoelectrodes with thin bubble plumes (e.g., vertical photoelectrodes) experience optical losses primarily due to surface-attached cap-shaped bubbles [10]. By contrast, for thicker plumes, the optical losses are governed mainly by the bubbles dispersed in the electrolyte.

4.6 Discussion

Overall, the results suggest that in order to minimize the optical losses, the bubble diameter D should be large, while the bubble volume fraction f_v and plume thickness H should be small. Thus, it is recommended that PEC cells be illuminated from the anode side to mitigate optical losses since oxygen bubbles are usually larger than hydrogen bubbles [28] (see Figure S7) and have half their volume fraction as per their stoichiometric ratios in water splitting reaction. Additionally, as per Fritz correlation [23], the bubble departure diameter

can be increased by increasing the surface tension γ_{eb} of the electrolyte/bubble interface. This can be achieved by decreasing the operating temperature of the PEC cell [29] and/or by increasing the concentration of salts in the electrolyte [30]. Additionally, the bubble departure diameter can be increased by increasing the bubble contact angle θ_c [23] on the photoelectrode. However, such a strategy increases optical losses due to backscattering at the bubble/photoelectrode interfaces. It also decreases the electrochemically active surface area of the photoelectrode [10, 31]. To address this, it is recommended to use a hydrophilic photoelectrode surface of contact angle $\theta_c \approx 20°$ which results in bubble departure diameter of around 1 mm at STP [23]. Such a bubble size would result in relatively low optical losses for a given gas generation rate.

The bubble-induced optical losses can be further mitigated by continuously removing the generated gas bubbles using forced convection in the electrolyte [4] which decreases both the bubble volume fraction f_v as well as the plume thickness H. The electrolyte layer should also be thin to minimize optical losses by absorption. However, the aqueous electrolyte must be readily available over the entire photoelectrode surface for water splitting to occur in the first place. In addition, the thickness of the electrolyte layer should not be too thin so as not to substantially increase the necessary pumping power. Therefore, the optimum electrolyte layer thickness corresponds to a compromise among optical losses, electrode performance, and process considerations.

One way to control the electrolyte layer thickness is to cover the photoelectrode with windows made of ultra-clear glass with anti-reflective coating that are highly transparent in the UV and visible wavelengths. Then, optical losses due to the presence of the window are negligible compared to those incurred by the presence of bubbles and by reflections at

the electrolyte/photoelectrode interface, as predicted in this study. Nishiyama et al. [32] presented such a design with arrangements to adjust the gap between the window and the photocatalyst sheet panels to as low as 100 µm. For such small thickness, the nucleated bubbles coalesced thus decreasing scattering losses.

The results also indicate that horizontal photoelectrodes suffer larger optical losses than vertical ones due to larger bubble plume thickness H (see Figure 1) for given bubble diameter D and volume fraction f_v. As a corollary, tilted photoelectrodes feature optical losses bounded by those for the horizontal and vertical orientations. Thus, the photoelectrode orientation should be optimized to maximize solar irradiation but also reduce the bubble plume thickness and thereby the optical losses.

4.7 Maximum achievable photovoltaic efficiency

Figure 8 plots the maximum achievable photovoltaic (PV) efficiency (%) as a function of bubble volume fraction f_v and plume thickness H for bubble diameter (a) $D = 1$ mm and (b) $D = 100$ µm, accounting for optical losses due to backscattering from bubbles in the electrolyte volume, absorption by the electrolyte, as well as reflections at the surface of a perfectly hydrophilic Si photoelectrode surface with no bubble coverage, i.e., $f_s = 0\%$. Indeed, accounting for the effect of surface-attached bubbles fell outside of the scope of the present study since the bubble coverage leads to local variations in the internal quantum efficiency in the photoelectrode causing some of the generated charge carriers to not participate in the redox reactions [17]. Figures 8(a) and 8(b) indicate that the maximum efficiency significantly decreases with decreasing bubble diameter and increasing volume fraction and/or

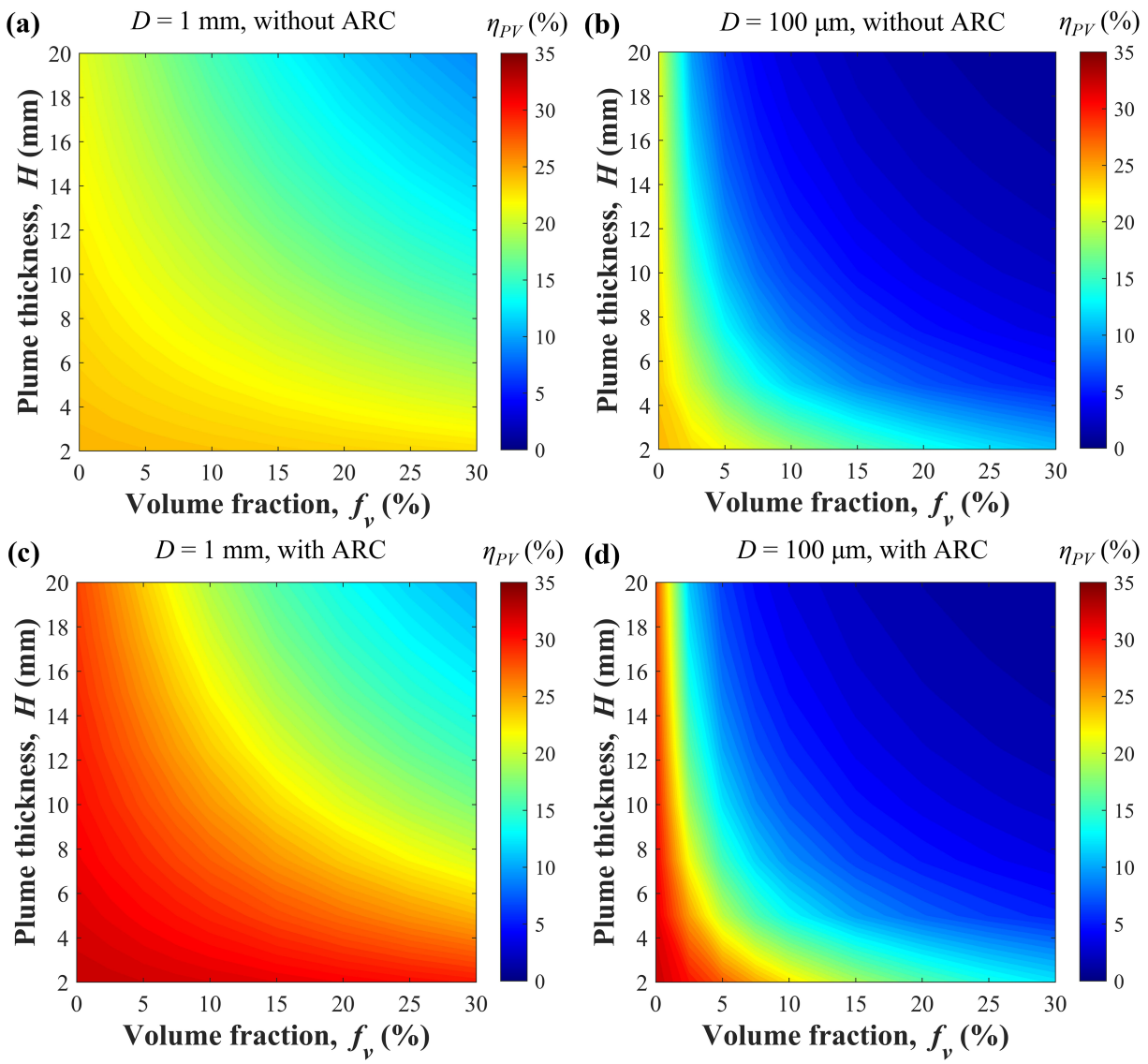

Figure 8: (a) Detailed-balance PV efficiency limit (%) incorporating bubble-induced optical losses for a Si photoelectrode immersed in a semitransparent aqueous electrolyte for bubble diameters (a) $D = 1$ mm and (b) $D = 100$ µm. The effect of using an antireflective coating (ARC) on the maximum achievable photoelectrode efficiency is also presented for bubble diameters (c) $D = 1$ mm and (d) $D = 100$ µm.

plume thickness due to increasing optical losses. For example, the PV efficiency limit at f_v = 10%, H = 10 mm, and D = 1 mm is about 20% compared with the efficiency limit of 33.5% for Si neglecting all optical losses. For small bubbles of diameter D = 100 µm, the efficiency limit was less than 10% for most plume thicknesses and volume fractions. In other words, optical losses can significantly reduce the photoelectrode performance.

One of the common ways to mitigate optical losses is to use an antireflective coating (ARC) on the photoelectrode surface. Typically for Si photoelectrodes, TiO_2 thin film can serve both as a protective and an antireflective coating [33, 34]. The effect of bubbles in such a scenario was investigated by assuming an idealized ARC-coated Si photoelectrode surface that was perfectly absorbing over the entire solar spectrum. The effect of ARC was computationally implemented by imposing the reflectance of the electrolyte/photoelectrode interface to be zero. Figures 8(c) and 8(d) plot the maximum achievable PV efficiency for ARC-coated Si photoelectrodes as a function of bubble volume fraction and plume thickness for bubble diameters D = 1 mm and 100 µm, respectively. Figures 8(c) and 8(d) demonstrate that the use of an antireflective coating increased the efficiency limits of the photoelectrode. However, the effect of bubbles on PV efficiency still remained significant, especially when the bubbles were small, resulting in large optical losses owing to multiple scattering of the incident rays by the bubbles. Overall, this study established that dealing with bubble-induced optical losses is an important issue to be addressed so as to achieve better photoelectrode performance in PEC cells.

5 Conclusion

This paper presented a comprehensive study to quantify the optical losses caused by the presence of non-absorbing gas bubbles in a semitransparent aqueous electrolyte as well as on the surface of a large Si photoelectrode. The Monte Carlo ray-tracing method was developed and validated to predict (i) the normal-hemispherical reflectance, (ii) the electrolyte absorptance, and (iii) the area-averaged absorptance of the photoelectrode for wavelengths between 400 and 1100 nm. The bubble diameter was found to most significantly affect the total optical losses, followed by the plume thickness, the bubble volume fraction, and the contact surface area coverage. Therefore, the bubble departure diameter should be increased to reduce the optical losses using strategies such as increasing the surface tension of the electrolyte/bubble interface by adding salts, for example. Similarly, the thickness of the bubble plume should be minimized by using shallow electrolyte layer and/or by flowing the electrolyte over the photoelectrode. The use of convection also decreases the bubble volume fraction thereby decreasing the optical losses arising from multiple scattering. The PEC cell should be illuminated from the anode size to mitigate optical losses since the oxygen bubbles have a larger diameter and smaller volume fraction as compared to hydrogen bubbles. Hydrophilic photoelectrode surface with bubble contact angle $\theta_c \approx 20°$ should be preferred to minimize the bubble contact surface area coverage and still ensure a large bubble departure diameter so as to minimize the optical losses. The use of an antireflective coating on a Si photoelectrode can enhance its performance for large bubbles. However, it is much less effective for high volume fraction of small bubbles since the photon flux reaching the photoelectrode decreases substantially due to bubble scattering. The conclusions reached in this study also apply

to tandem configurations where the incident light inevitably interacts with bubbles. The trends reported for efficiency should be qualitatively the same despite the lower transmitted light intensity and the different bandgaps of materials. Overall, significant optical losses incurred at high gas generation rates can prove detrimental to the commercial viability of water splitting in PEC cells. Thus, careful design and operation to control bubble size and ensure fast bubble removal is important.

Conflicts of Interest

There are no conflicts of interest to declare.

CRediT authorship contribution statement

Abhinav Bhanawat: Conceptualization, Methodology, Validation, Software, Formal Analysis, Investigation, Visualization, Writing - Original Draft, Writing- Reviewing and Editing. Laurent Pilon: Supervision, Conceptualization, Writing- Reviewing and Editing, Funding Acquisition.

Acknowledgment

This study was supported, in part, by the National Science Foundation NRT-INFEWS: Integrated Urban Solutions for Food, Energy, and Water Management (Grant No. DGE-1735325). This work used computational and storage services associated with the Hoffman2 Shared Cluster provided by UCLA Institute for Digital Research and Education's Research

Technology Group. Abhinav Bhanawat is grateful to the UCLA Mechanical and Aerospace Engineering Department for financial support through a graduate research fellowship.

References

[1] N. S. Lewis, "Research opportunities to advance solar energy utilization," *Science*, vol. 351, no. 6271, p. aad1920, 2016.

[2] J. Barber, "Hydrogen derived from water as a sustainable solar fuel: learning from biology," *Sustainable Energy & Fuels*, vol. 2, no. 5, pp. 927–935, 2018.

[3] J. H. Kim, D. Hansora, P. Sharma, J.-W. Jang, and J. S. Lee, "Toward practical solar hydrogen production–an artificial photosynthetic leaf-to-farm challenge," *Chemical Society Reviews*, vol. 48, no. 7, pp. 1908–1971, 2019.

[4] A. Angulo, P. van der Linde, H. Gardeniers, M. Modestino, and D. F. Rivas, "Influence of bubbles on the energy conversion efficiency of electrochemical reactors," *Joule*, vol. 4, no. 3, pp. 555–579, 2020.

[5] M. A. Modestino, S. M. H. Hashemi, and S. Haussener, "Mass transport aspects of electrochemical solar-hydrogen generation," *Energy & Environmental Science*, vol. 9, no. 5, pp. 1533–1551, 2016.

[6] Y. Liang, T. Tsubota, L. P. Mooij, and R. van de Krol, "Highly improved quantum efficiencies for thin film $BiVO_4$ photoanodes," *The Journal of Physical Chemistry C*, vol. 115, no. 35, pp. 17594–17598, 2011.

[7] J. Saari, H. Ali-Loytty, M. Honkanen, A. Tukiainen, K. Lahtonen, and M. Valden, "Interface engineering of TiO_2 photoelectrode coatings grown by atomic layer deposition on silicon," *ACS Omega*, vol. 6, no. 41, pp. 27501–27509, 2021.

[8] J.-H. Kim, D. H. Kim, J. W. Yoon, Z. Dai, and J.-H. Lee, "Rational design of branched WO_3 nanorods decorated with $BiVO_4$ nanoparticles by all-solution processing for efficient photoelectrochemical water splitting," *ACS Applied Energy Materials*, vol. 2, no. 6, pp. 4535–4543, 2019.

[9] Q. Chen, G. Fan, H. Fu, Z. Li, and Z. Zou, "Tandem photoelectrochemical cells for solar water splitting," *Advances in Physics: X*, vol. 3, no. 1, p. 1487267, 2018.

[10] A. Bhanawat, K. Zhu, and L. Pilon, "How do bubbles affect light absorption in photoelectrodes for solar water splitting?," *Sustainable Energy & Fuels*, vol. 6, no. 3, pp. 910–924, 2022.

[11] M. F. Modest and S. Mazumder, *Radiative Heat Transfer*. 4th ed., Academic Press, New York, NY, 2021.

[12] J. R. Howell, M. P. Mengüç, K. Daun, and R. Siegel, *Thermal Radiation Heat Transfer*. 7th ed., CRC Press, Boca Raton, FL, 2020.

[13] P. A. Kempler, Z. P. Ifkovits, W. Yu, A. I. Carim, and N. S. Lewis, "Optical and electrochemical effects of H_2 and O_2 bubbles at upward-facing Si photoelectrodes," *Energy & Environmental Science*, vol. 14, no. 1, pp. 414–423, 2021.

[14] H. Döscher, J. Geisz, T. Deutsch, and J. Turner, "Sunlight absorption in water–efficiency and design implications for photoelectrochemical devices," *Energy & Environmental Science*, vol. 7, no. 9, pp. 2951–2956, 2014.

[15] W. Shockley and H. J. Queisser, "Detailed balance limit of efficiency of p-n junction solar cells," *Journal of Applied Physics*, vol. 32, no. 3, pp. 510–519, 1961.

[16] C. H. Henry, "Limiting efficiencies of ideal single and multiple energy gap terrestrial solar cells," *Journal of Applied Physics*, vol. 51, no. 8, pp. 4494–4500, 1980.

[17] A. E. Dorfi, A. C. West, and D. V. Esposito, "Quantifying losses in photoelectrode performance due to single hydrogen bubbles," *The Journal of Physical Chemistry C*, vol. 121, no. 48, pp. 26587–26597, 2017.

[18] I. Holmes-Gentle, F. Bedoya-Lora, F. Alhersh, and K. Hellgardt, "Optical losses at gas evolving photoelectrodes: implications for photoelectrochemical water splitting," *The Journal of Physical Chemistry C*, vol. 123, no. 1, pp. 17–28, 2018.

[19] R. L. Curl, "Note on light transmission through a polydisperse dispersion," *AIChE Journal*, vol. 20, no. 1, p. 184, 1974.

[20] F. Njoka, S. Mori, S. Ookawara, and M. Ahmed, "Effects of photo-generated gas bubbles on the performance of tandem photoelectrochemical reactors for hydrogen production," *International Journal of Hydrogen Energy*, vol. 44, no. 21, pp. 10286–10300, 2019.

[21] G. M. Hale and M. R. Querry, "Optical constants of water in the 200-nm to 200-μm wavelength region," *Applied Optics*, vol. 12, no. 3, pp. 555–563, 1973.

[22] M. A. Green, "Self-consistent optical parameters of intrinsic silicon at 300 K including temperature coefficients," *Solar Energy Materials and Solar Cells*, vol. 92, no. 11, pp. 1305–1310, 2008.

[23] V. P. Carey, *Liquid-Vapor Phase-Change Phenomena.* 3rd ed., CRC Press, Boca Raton, FL, 2020.

[24] K. Zhu, Y. Huang, J. Pruvost, J. Legrand, and L. Pilon, "Transmittance of transparent windows with non-absorbing cap-shaped droplets condensed on their backside," *Journal of Quantitative Spectroscopy and Radiative Transfer*, vol. 194, pp. 98–107, 2017.

[25] H. Dotan, N. Mathews, T. Hisatomi, M. Grätzel, and A. Rothschild, "On the solar to hydrogen conversion efficiency of photoelectrodes for water splitting," *The Journal of Physical Chemistry Letters*, vol. 5, no. 19, pp. 3330–3334, 2014.

[26] W. Yang, R. R. Prabhakar, J. Tan, S. D. Tilley, and J. Moon, "Strategies for enhancing the photocurrent, photovoltage, and stability of photoelectrodes for photoelectrochemical water splitting," *Chemical Society Reviews*, vol. 48, no. 19, pp. 4979–5015, 2019.

[27] I. Holmes-Gentle and K. Hellgardt, "A versatile open-source analysis of the limiting efficiency of photo electrochemical water-splitting," *Scientific Reports*, vol. 8, no. 1, pp. 1–9, 2018.

[28] K. Matsuura, Y. Yamanishi, C. Guan, and S. Yanase, "Control of hydrogen bubble plume during electrolysis of water," *Journal of Physics Communications*, vol. 3, no. 3, p. 035012, 2019.

[29] K. Ali, A. A. Shah, S. Bilal, and A. A. Shah, "Surface tensions and thermodynamic parameters of surface formation of aqueous salt solutions: III. Aqueous solution of KCl, KBr and KI," *Colloids and Surfaces A: Physicochemical and Engineering Aspects*, vol. 337, no. 1, pp. 194–199, 2009.

[30] M. Sadeghi, V. Taghikhani, and C. Ghotbi, "Measurement and correlation of surface tension for single aqueous electrolyte solutions," *International Journal of Thermophysics*, vol. 31, no. 4, pp. 852–859, 2010.

[31] K. Obata and F. Abdi, "Bubble-induced convection stabilizes local pH during solar water splitting in neutral pH electrolytes," *Sustainable Energy & Fuels*, vol. 5, no. 15, pp. 3791–3801, 2021.

[32] H. Nishiyama, T. Yamada, M. Nakabayashi, Y. Maehara, M. Yamaguchi, Y. Kuromiya, Y. Nagatsuma, H. Tokudome, S. Akiyama, T. Watanabe, *et al.*, "Photocatalytic solar hydrogen production from water on a 100-m^2 scale," *Nature*, vol. 598, no. 7880, pp. 304–307, 2021.

[33] B. Seger, T. Pedersen, A. B. Laursen, P. C. Vesborg, O. Hansen, and I. Chorkendorff, "Using TiO_2 as a conductive protective layer for photocathodic H_2 evolution," *Journal of the American Chemical Society*, vol. 135, no. 3, pp. 1057–1064, 2013.

[34] W.-H. Cheng, M. H. Richter, M. M. May, J. Ohlmann, D. Lackner, F. Dimroth, T. Hannappel, H. A. Atwater, and H.-J. Lewerenz, "Monolithic photoelectrochemical device for direct water splitting with 19% efficiency," *ACS Energy Letters*, vol. 3, no. 8, pp. 1795–1800, 2018.